# Solute influence in transitions from non-Arrhenius to stick-slip Arrhenius grain boundary migration

Akarsh Verma<sup>1,3</sup>, Oliver K. Johnson<sup>1</sup>, Gregory B. Thompson<sup>2</sup>, Shigenobu Ogata<sup>3</sup>, and Eric R. Homer<sup>1\*</sup>

<sup>1</sup> Department of Mechanical Engineering, Brigham Young University, Provo, UT, USA

<sup>2</sup> Department of Metallurgical and Materials Engineering, The University of Alabama, Tuscaloosa, AL, USA

<sup>3</sup> Department of Mechanical Science and Bioengineering, Graduate School of Engineering Science, Osaka University, Osaka, Japan

\*Corresponding author E-mail address: eric.homer@byu.edu (Eric R. Homer)

#### **Abstract**

Synthetic driving force based molecular dynamics simulations are used to evaluate the grain boundary (GB) velocities for an incoherent  $\Sigma 3$  [111] 60° {11 8 5} GB in elemental nickel and its copper-based alloys. The effects of temperature, solute content, and magnitude of the driving force on GB velocity trends along with the mechanisms acting behind them are reported. We observe that, for pure nickel and its copper alloys at high driving forces, these special GBs exhibit non-Arrhenius or anti-thermal migration behavior, where temperature and GB velocity are inversely related. For lower driving forces, the increased copper content leads to stick-slip migration behavior and a likely transition from non-Arrhenius to Arrhenius temperature dependence. Interestingly, the ordered atomic motions are frustrated but unchanged by the solute content and stick-slip migration. While the results are generally consistent with the Cahn-Lücke-Stüwe (CLS) model, no solute drag is observed; rather, the solute effects are likely the result of solute pinning.

**Keywords:** Grain boundary migration, Molecular dynamics, Nickel, Copper, Alloys, Solute resistance, Stick-Slip

#### 1 Introduction

It is well known that grain growth is expected at elevated temperatures, but experiments have also confirmed stress driven coarsening taking place at cryogenic temperatures [1-5]. For instance, Brons et al. [2] reported grain growth in nano-twinned indented copper (Cu) while being immersed in a liquid nitrogen environment. More recently, Robinson et al. [6] experimentally reported how solutes can impact this cryogenic coarsening. In this work, they reported a variation of responses depending on the solute content and the stress field from the indenter impression into the material. In this paper, we seek to better understand the effect of solute concentration on cryogenic boundary migration in face centered cubic (FCC) metals.

Traditionally, GB migration is believed to occur through either thermally activated process at the atomic level or by gliding of the constituent dislocations [7]. In thermally activated migration, a GB will migrate at a velocity, v, proportional to the driving force, p, applied to the boundary according to

$$v = Mp \tag{1}$$

where the proportionality factor, M, is defined as the mobility. The mobility is typically given by the Arrhenius relationship

$$M = M_o e^{-(Q/k_B T)}$$
 (2)

where  $M_o$  is a constant pre-exponential factor, Q is activation energy (or intrinsic barrier height of migration),  $k_B$  is the Boltzmann constant, and T is temperature. According to equation 2, GB mobility should exponentially increase with the temperature.

However, computational results have predicted that GB mobilities are not always positively correlated with temperature [8-13]. For instance, incoherent  $\Sigma 3$  GBs (and some  $\Sigma 7$  as well as  $\Sigma 9$  GBs) exhibit non-Arrhenius (antithermal) behavior, where mobility and temperature are negatively correlated with each other [9-13]. Homer et al. [14] have shown that a classical migration model can account for and predict the full spectrum of antithermal to Arrhenius migration behaviors. This classical model serves as the origin to equations 1 and 2 and is given by

$$v = v_o \exp\left(-\frac{Q}{k_B T}\right) 2 \sinh\left(\frac{p}{2k_B T}\right)$$
 (3)

Equation 3 produces identical results to equations 1 and 2 when Q is large and  $p \ll k_B T$ , which corresponds to Arrhenius temperature dependence. However, when Q is small, the form of the sinh term leads to non-Arrhenius temperature dependence. Further discussion on this classical model is provided in [14] where it includes a discussion on how this classical model can account for cryogenic and non-Arrhenius migration behaviors observed in both experiments and simulations.

Interestingly, the cryogenic boundary migration observed in simulations all involve synchronous, ordered atomic motions [10, 12, 13, 15, 16]. These coordinated motions occur in such a manner that each atom has a specific direction it will move relative to its neighbors. In fact, part of the reason for the non-Arrhenius boundary migration among these GBs is that thermal energy frustrates, rather than helps, the coordinated atomic motions. However, a question remains about how solute atoms, or point defects, might disrupt the ordered motions central to the cryogenic migration. It is unclear if atoms that are chemically distinct from each other but occupy the same

lattice site would have an invariant effect to this required motion. Elucidating this behavior would then enable the ability to chemically engineer the fundamental mechanisms of cryogenic growth.

Ni and Cu are both FCC metals with similar atomic radii and masses yielding comparable elastic effects, which supports it forming a solid solution at elevated temperatures. At low temperatures a miscibility gap does exist, but the enthalpy of mixing is only slightly positive [17, 18]. As a result, the thermodynamic driving force for separation is low. In addition, the peak miscibility gap temperature is less than 1/3 the homologous temperature, making it kinetically difficult for the atoms to partition. Nevertheless, nanocrystalline samples near 50 at.% Cu have shown a miscibility gap around 500°C [19] where the higher concentration results in a higher driving force. Electrodeposited nanocrystalline samples with composition values in the 12-44 at.% Cu have shown a Cu-rich GB phase form after annealing at 575 K, but these may form from segregation or the Cu seed layer below the thin film [20]. In the dilute limit, one can expect that such partitioning would be more limited and that a copper atom can site substitute for nickel with only a modest tendency to partition.

Solute influence on GB growth has been a topic of research for several decades [7, 21, 22] and is well described by the Cahn-Lücke-Stüwe (CLS) model [23, 24]. In the solute drag model, the solute will aggregate at the boundary, either through prior segregation or accumulation during migration, leading to a drag effect and subsequent slowing of the migration. Various molecular dynamics studies have shown that as the solute content increases, the boundary velocity decreases which is in accordance with this conventional CLS model [25-28]. Koju and Mishin show clear evidence can be seen in the effect of solute drag on the boundary as well as faster

migration when the boundary can break away from the solute atoms [25]. More recently, Hersent et al. [29] have suggested in a solute pinning model where the rate limiting step is the jumping of atoms out of the boundary. Furthermore, special GBs have been shown to exhibit different characteristics [23, 25] from high angle random boundaries, assumed to be the basis for the CLS model.

Here, we propose to use the Ni-Cu alloy to examine the effects of solute atoms on the migration behavior of an incoherent twin boundary that has been previously reported to exhibit non-Arrhenius behavior [8, 11, 13, 14, 16, 30]. We utilize synthetic driving force based molecular dynamics simulations to evaluate the GB velocities for a Ni GB with different levels of Cu solute over a range of temperatures and driving forces. The simulation results are examined to see how the solute atoms affect the characteristic migration behaviors of this boundary, including the impact of the solute atoms on the coordinated atomic motions and on the tendency of the solute atoms to stay in lattice sites vs. partitioning to and migrating with the boundary.

#### 2 Methods

The (11 8 5)/(8 11 5) incoherent twin ( $\Sigma$ 3) GB in this work has been studied extensively for its non-Arrhenius behaviors [8, 11, 13, 14, 16, 30]. This work is mainly focused on the migration behavior of this GB in pure Ni and Ni-Cu alloys. We have utilized the embedded atom method (EAM) potential developed by Fischer et al. [31] to capture the interactions between Ni and Cu atoms. This potential was developed to study the GB formation energy and dynamics in a Ni-Cu alloy, making it ideal for GB migration simulations in this alloy system. Fully periodic bi-crystal simulation cells with a box size of 104 (x-direction)  $\times$  86 (y-direction)  $\times$  408 Å<sup>3</sup> (z-direction)

(comprising of approximately 335800 atoms) were constructed using standard methods [32-35]. Here GBs are present in the x-y plane, and we measure the migration normal to the boundary plane (z-direction); a schematic of the bicrystal and GB structure is presented in supplemental Figure S1a. The minimum energy configuration was obtained using the conjugate gradient algorithm. Each simulation cell was equilibrated for 60 ps to ensure temperature convergence to a desired value of 50, 100, 200, 300, 600, 1000, or 1400 K, and relaxed to a desired pressure of 0 MPa. The molecular dynamics simulations used the Large-scale Atomic/Molecular Massively Parallel Simulator (LAMMPS) package [36] and post-processing was performed with the help of the Open Visualization Tool (OVITO) software [37].

As noted above, Ni and Cu form a substitutional solid solution [38-40] with a low driving force to partition in the dilute limit. Various molecular dynamics studies have examined Ni and Cu based alloys with random replacement of atoms (e.g. no segregation) [40, 41-43]. To verify that we should not expect segregation, we performed Monte Carlo (MC) swaps of Cu and Ni atoms to look for segregation or preferred sites. A simulation with 20,000 MC swaps was carried out for a 6 at % Cu sample at both 50 K and 600 K. The MC swaps show no indication of segregation to or away from this particular GB, as illustrated in supplemental Figure S1. As a result, Cu atoms were randomly and uniformly distributed throughout the bi-crystalline Ni domain, as in [40, 41], to achieve the desired Ni-Cu alloy with effective concentrations of 2, 4, 6, 8 and 10 at. % Cu. These concentrations are referred to as NiCu0, NiCu2, NiCu4, NiCu6, NiCu8, and NiCu10 in this work, where the numeric value represents the respective at. % of Cu in Ni.

The energy conserving orientational (ECO) force method [44, 45] was used to induce boundary migration at three driving force values (0.001, 0.005, and 0.010 eV/atom). Since the time scale is

comparatively lower than those of experiments, the driving force is high in comparison to those found in typical experimental conditions [16, 46]. This ECO driving force utilizes an orientation parameter, which allows the method to add or subtract energy from atoms depending on which of the two grains they are in. This energy difference causes atoms in the higher energy grain to attach to the lower energy grain, which lowers the system energy and causes GB migration. The ECO force threshold order parameter ( $\eta$ ) was taken to be 0.25, and a cutoff radius of 1.1 times the lattice parameters was selected [16]. For every simulation conducted, the GB was subjected to the ECO driving force until the two grains coalesced to form a single grain (a complete sweep by the GBs) or for a maximum of 1000 ps.

The GB velocity is computed from the GB position vs. time data, tracked independently for the two GBs in each simulation cell. The GB position at a given time step is defined as the mean z-position of all atoms belonging to the GB, as defined by atoms not belonging to either grain in the ECO driving force calculations  $(-1 < \chi < 1)$ . To account for the fact that not all GB position vs. time data are linear over the entire duration of the simulation, the authors employed a temporal subdivision method to fit the velocity over periods of 10 ps [47]. This enables characterization of the velocity even under stick-slip migration conditions to capture both the stationary and migrating behaviors. Therefore, at any given temperature, we obtain a distribution of velocities, providing a measure of uncertainty in GB migration measurements.

In the analysis of the atomic motions, the relative atomic motions of the atoms as the GB sweeps through have been calculated using the slip vector analysis from Zimmerman et al. [48]. In these plots, the relative atomic motions are shown from a common origin to illustrate the ordered nature of the motions as well as the scatter induced by additional thermal energy [49].

# 3 Results

Figure 1 plots the median value of the velocity distribution with error bars showing the interquartile range of the distribution; the full distributions are plotted in supplementary Figure S2. One of the first things to notice in Figure 1 is that the GB velocity values decrease as solute % increases for all driving forces. This is unsurprising given the present understanding of the impact of solute atoms on GB migration, and similar inverse relationships between GB velocity and that solute concentration have already been observed for high solute concentrations of Cu in Ni for  $\Sigma$ 9 tilt symmetric GBs [41].

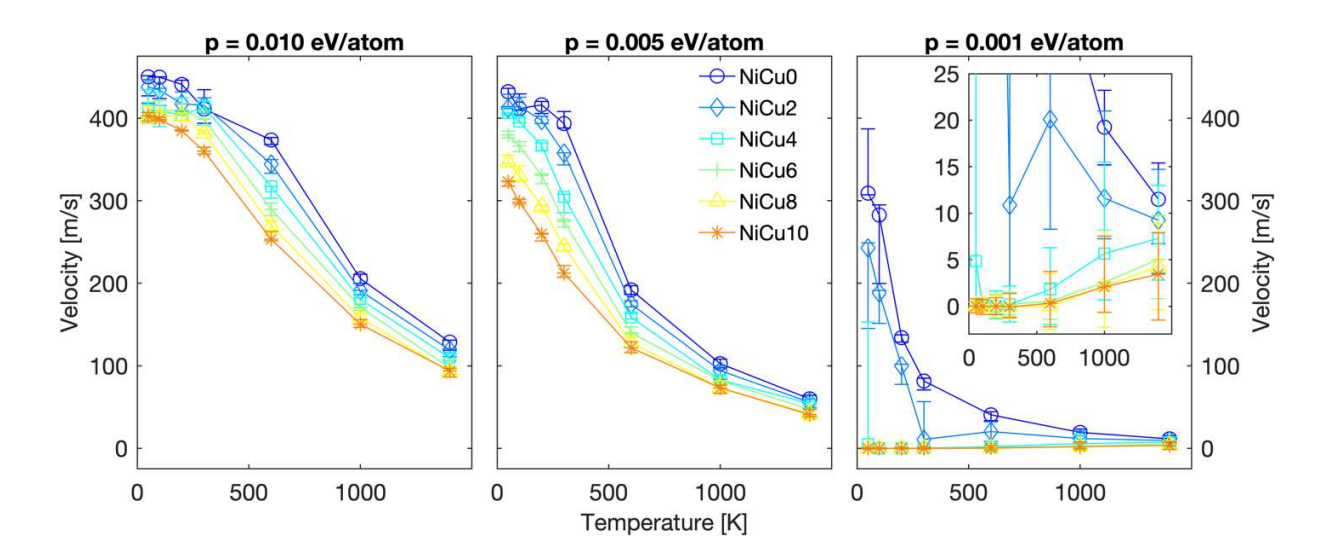


**Figure 1.** GB velocity as a function of temperature for different synthetic driving forces and solute content. The marker shows the median velocity value and error bars show the 1<sup>st</sup> and 3<sup>rd</sup> quartiles of the full velocity distributions shown in the supplemental Figure S2. The lines connecting the data points are included only to guide the eye.

From Figure 1, it is also clear that at higher driving forces (0.010 and 0.005 eV/atom) both Ni and Ni-Cu alloys exhibit an inverse relationship between temperature and GB velocity, which

can be characterized as non-Arrhenius. At a low driving force of 0.001 eV/atom, there is considerably more variation in the velocity behaviors. The pure Ni (NiCu0) configuration exhibits decreasing velocity values with increasing temperature. In contrast, at higher alloy content (6-10 at. % Cu), the median velocity values are much lower and seem to increase slightly with temperature, with a noted large range of velocity values (relative to the median) as given by the range of the quartile values in the plot, which can be seen more clearly in the inset to Figure 1 at the 0.001 eV/atom driving force. The two simulations with intermediate alloy compositions (NiCu2 and NiCu4), exhibit fast migration at low temperatures, but the velocity variation is more erratic. Regardless, at these lower driving forces and higher solute content, the very fast non-Arrhenius migration is frustrated, and the temperature dependence of the trend is altered as a result. While the large distribution of velocity values at the higher solute content and low driving force makes it difficult to state this with certainty, it is possible that non-Arrhenius-type migration is transitioning to Arrhenius-type migration as a result of this change. Signatures of this possible transition can even be observed in the NiCu4 configuration where the GBs exhibit non-Arrhenius migration at lower temperatures only (< 300 K), and then seem to exhibit Arrhenius-type behavior as the temperature increases. Song and Deng [50] have recently predicted a transition from thermally activated to non-thermally activated behavior in Ni as a function of driving force only, when driving forces become extremely small. This possible interpretation is discussed in more detail in section 4.4.

Comparison of the data to the model in equation 3 requires characterization of which temperature and driving force conditions fall within its range of applicability. To accomplish this, we first plot the same median velocities divided by the magnitude of the driving force,  $\nu/p$ , as a function of temperature. This is illustrated in Figure 2, where the data are categorized by solute content

rather than the driving force. Under certain conditions, the data deviates from the model significantly because of two effects that will be described shortly.

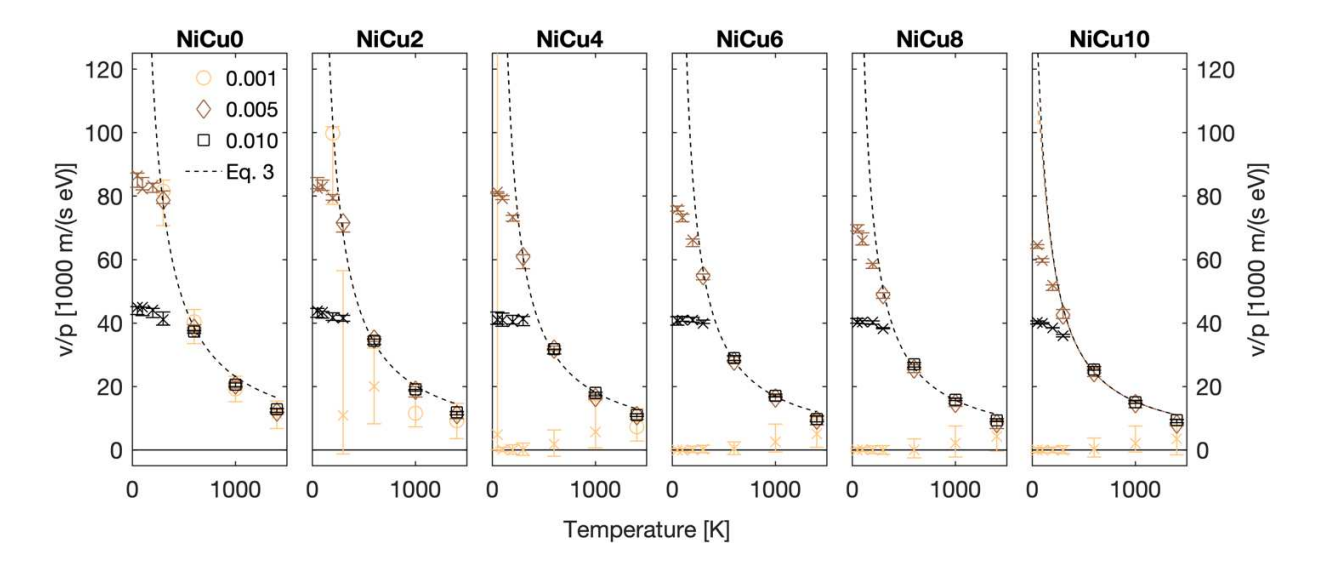


**Figure 2.** Plots showing GB velocity/driving force vs. temperature trend for different configurations and synthetic driving forces. The marker shows the median velocity value and error bars show the 1<sup>st</sup> and 3<sup>rd</sup> quartiles of the full velocity distributions shown in supplemental Figure S2. The legend lists the driving forces in eV/atom. The horizontal black line at v/p = 0 is added to guide the eye.

Figure 2 includes a fit to equation 3 using a subset of the datapoints that fall within the model's range of applicability. The selection of which points to include (which defines the range of applicability) used the following method. Starting with and always including the three highest temperatures at the two highest driving forces (which are consistently non-Arrhenius), an iterative procedure was employed to determine the best fit of these points to equation 3. But, in each iteration, if the model prediction fit fell between the 1<sup>st</sup> and 3<sup>rd</sup> quartiles of the velocity distribution at a given temperature, those values were included in the subsequent fit iteration.

The iterative fitting procedure continued until there were no changes from one iteration to the next. The values not included in the final fitting are marked with an 'x' in Figure 2.

It can be seen in Figure 2 that many of the datapoints, including simulations at different driving forces, have identical w/p ratios and conform to the predictions of equation 3. This is evident when the markers fall on top of each other and the dotted line at the higher temperatures and for all but the lowest driving force. Thus, both the model and the simulations at different driving forces all predict the same w/p ratio, which corresponds to the mobility, M, in the traditional definition of equation 2. This correspondence between points even at different driving forces makes it easier to identify the deviations from equation 3 that occur under certain conditions. These deviations can be explained by two phenomena observed previously in GB migration. The first is a velocity saturation where a GB reaches a terminal velocity of sorts at high driving forces and low temperatures [10, 51, 52]. The second is 'stick-slip' behavior where a GB exhibits stop and go motion [53] observed in this work at lower driving forces and higher solute content. The characteristics of these deviations are examined further in the discussion section.

## 4 Discussion

The discussion is organized as follows: First, we describe the characteristics of the velocity saturation observed in this work. This is followed by a discussion of the characteristics of the simulations that follow non-Arrhenius migration. The characteristics of the simulations that exhibit stick-slip behavior are then discussed. These are all followed by a discussion of how solute content effects the observed migration in these simulations.

#### 4.1 Velocity saturation

The phenomenon of velocity saturation has been reported for GB migration [10, 52] and mirrors the behavior of dislocation motion, where under certain conditions, the dislocation cannot migrate faster than a forbidden velocity [51]. This phenomenon is most easily seen in a plot of the velocity as a function of the ratio of driving force over thermal energy,  $p/k_BT$ . The same data from Figures 1 and 2 are presented in this way in Figure 3. It can be seen here that, except for the lowest driving force where we see stick-slip behavior (discussed later), the rest of the data follow a characteristic trend. Here, the GB velocity is directly proportional to  $p/k_BT$  for low values of  $p/k_BT$  (that is essentially dominated by high temperatures). But this direct proportional relationship breaks down when the GB velocity reaches some saturation value and becomes constant and independent of  $p/k_BT$ . Consequently, at lower temperatures and higher driving forces, one cannot continue to induce an acceleration in the velocity of the GB as it reaches a terminal or forbidden velocity.

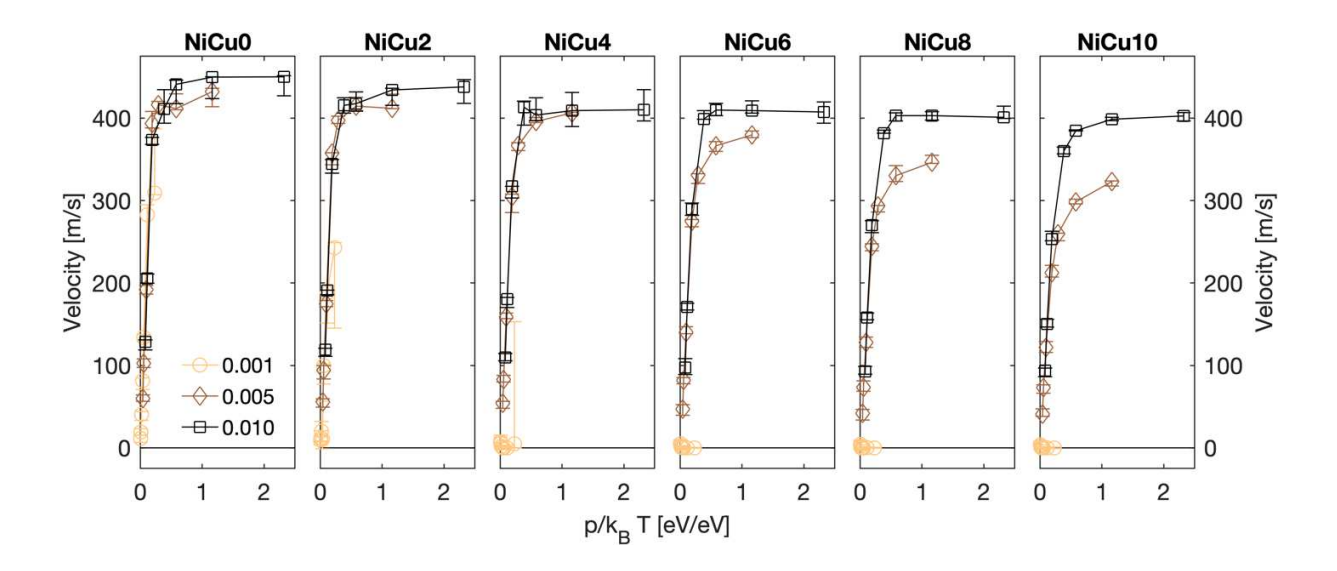


**Figure 3.** Plots showing GB velocity vs thermal energy  $(p/k_B T)$  trend for different configurations and synthetic driving forces. The marker shows the median velocity value and error bars show the 1<sup>st</sup> and 3<sup>rd</sup> quartiles of the velocity distributions shown in supplemental Figure S2. The legend lists the driving forces in eV/atom. The lines connecting the data points and the horizontal black line at v = 0 are included only to guide the eye.

The saturation velocity decreases with increasing solute content and appears to be dependent on driving force at higher solute content. In dislocation motion, the forbidden velocity is related to the wave speed in the material [51]. However, a recent examination of this phenomenon using seven different interatomic potentials to simulate GB migration found no correlation between the saturation velocity and the elastic constants, nor with several other properties calculated for those potentials [52]. The atomic motions appear to be the same below and above the saturation velocity, which can be seen in the supplemental Figure S3.

The results in this work do not explain what controls the velocity saturation. In fact, the dependence of the velocity saturation value on solute content and, in the case of high solute contents, on driving force as well, only adds to the mystery. Because this phenomenon is not of central interest to this work, we leave this unresolved question for future work. However, given that this velocity saturation has been observed previously and can explain why the velocity values deviate from the model in equation 3 at high driving forces and low temperatures, it is now clear why these particular simulations did not conform to equation 3; the model simply predicts faster velocity values than are allowed.

### 4.2 Non-Arrhenius boundary migration

To discuss those simulations that exhibit non-Arrhenius GB migration, we refer to the simulations in Figure 2 that follow the model based on predictions from equation 3. The characteristics of this phenomenon have been investigated and described in numerous works [8, 10-13, 15, 16, 49, 50, 54]. These characteristics are that ordered atomic motions appear to be a necessary condition to observe non-Arrhenius migration, and that the ordered motions are frustrated rather than facilitated by the increase of temperature. This thermal disordering caused by the additional thermal energy [55] hinders the ordered atomic shuffling and imparts more irregularity in the system leading to slower migration at higher temperatures. The effect can be seen in (i) a scattering of the ordered atomic motions and (ii) GBs exhibiting short periods of time when they migrate backwards or not at all. Both detract from the forwards migration of the boundary and lead to decreased velocity with increased temperature. These two signatures can be seen for the 0.010 eV/atom driving force in the present work in supplemental Figures S3 and S4, respectively. Note that in supplemental Figure S4, the boundary migrates backwards for short periods of time at the highest temperature. This type of behavior is predicted by the migration model of equation 3 when the barrier height to migration is small and additional thermal energy does little to help the forwards events but increases the frequency of the backwards events, resulting in slower velocity predictions at higher temperatures and an overall behavior that is non-Arrhenius [14].

Another key characteristic of non-Arrhenius migration is faceting. Chesser and Holm noted that since this particular GB ( $\Sigma$ 3 (11 8 5)) migrates by the motion of the three Shockley partial triplets, all the equilibrium facets come in multiples of three {111} planes [13]. They also noted

that coalescence of small facets into a larger facet appears to be a necessary but insufficient condition for the non-Arrhenius migration behavior.

In the present work, we have observed a temperature dependence in the faceting behavior. As illustrated in Figure 4, the facet becomes rougher with increasing temperature. This planar facet disappearance (decreasing of facet length) or roughening (defaceting) with rising temperature is well documented [56-59] and has been observed in  $\Sigma 3$  GBs in bi-crystal copper as well [60]. It is also accepted that a rough boundary will migrate more quickly than a smooth boundary [11, 61]. However, the roughening of this flat boundary appears to frustrate the migration of the Shockley partial triplets and separate the large facets into several smaller facets, whose coalescence was listed as a necessary condition for non-Arrhenius boundary migration [13]. This may be another key characteristic caused by the thermal disorder of increased temperature.

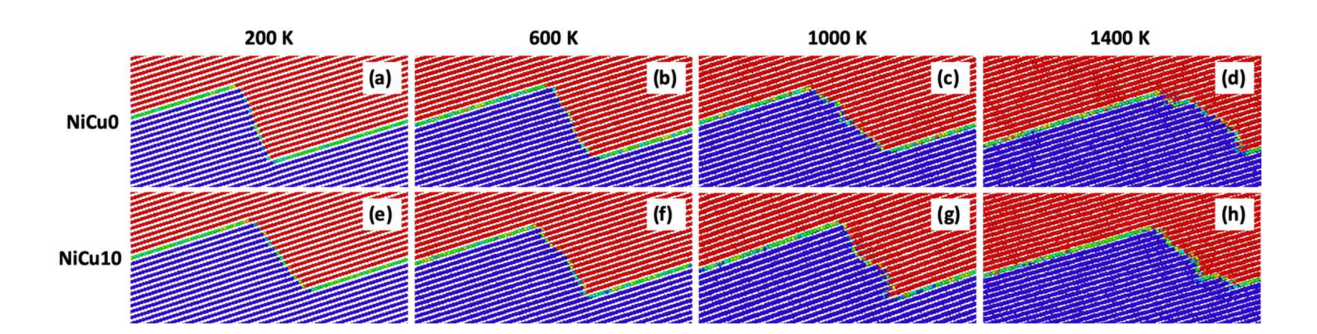


**Figure 4.** Snapshots of GB movement at 0.010 eV/atom driving force for (a-d) NiCu0, and (e-h) NiCu10 alloy configuration (Red and blue colored atoms signify the grains domain).

Since faceted GBs migrate differently than the smooth ones [62], it may be that roughening has different effects in the migration of flat and faceted boundaries. For facets that migrate quickly by ordered atomic motions through step flow, the roughening may simply frustrate this process, thereby decreasing the GB migration velocity. In contrast, for a smooth, flat GB, roughening is

expected to accelerate the growth of the boundary [55]. This assertion that roughening can slow boundary migration will require further evidence but could be important in understanding the conditions for boundaries that could exhibit non-Arrhenius GB migration. In general, faceted GBs are believed to move with low mobility [63], but a few works have reported highly mobile facets [57, 61] and a correlation between facet length and facet mobility [57, 64].

To show the effect of solute concentration, one can see in Figure 1 that added solute content clearly slows the migration. As seen in Figure 2, equation 3 captures the non-Arrhenius migration well for the range of solute considered, allowing us to see how the model parameters for equation 3 vary with solute content. Figure 5 shows the velocity prefactor,  $v_o$ , and migration barrier, Q, values obtained from the fits as a function of Cu solute content. The change of  $v_o$  and Q with composition corresponds to decreased migration velocities with increased solute content, though Q only increases above negligibly small values at the highest solute contents. From a model perspective, this would suggest that increased solute content is making the migration barrier larger, which makes physical sense since an atom of a different size would frustrate the coordinated motion of the surrounding atoms. As described in [14], Q values above ~0.1 eV are sufficiently high that non-Arrhenius migration is unlikely to be observed. Thus, while non-Arrhenius migration is still observed in the NiCu10 case examined here, the trend of the highest values of Q in Figure 5 suggest non-Arrhenius migration is unlikely to be observed at compositions higher than 15 at. %.

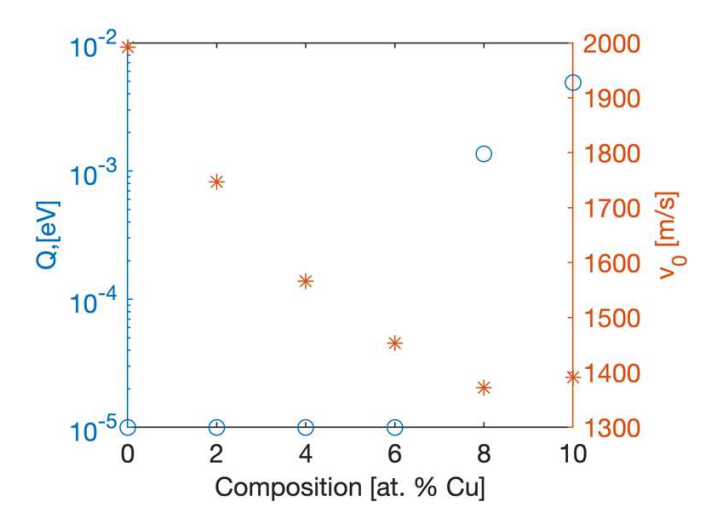


**Figure 5.** Fit parameters for the barrier height of migration (Q) and velocity prefactor  $(v_o)$  from equation 3 as function of solute content.

The velocity prefactor,  $v_o$ , decreases by ~30% from NiCu0 to NiCu10. Factors that could contribute to this change would be the Debye frequency of the atoms involved in the process as well as the jump distance experienced by the atoms. Since the fitting variables capture the collective behavior of the process, there is no one value for these properties. Perhaps the different elastic constants or bond lengths between the Ni and Cu atoms frustrate the migration leading to smaller  $v_o$  values.

It is worth noting that the Q values are more sensitive to the fitting procedure than  $v_o$  is. A change in which points are included in the fitting is therefore likely to have a large effect on any changes in the Q values, though the general trends are not affected too much. In short,  $v_o$  decreases with increasing solute content and Q values experience some slight increase at higher solute content but consistently remain small enough to predict non-Arrhenius migration for the range of solute concentrations considered here.

#### 4.3 Stick-Slip Migration

As noted in Section 3 and as illustrated in Figures 1 and 2, many of the simulations had velocity values that did not conform to the predictions from equation 3 at the lowest driving force of 0.001 eV/atom. It was noted that the deviation from equation 3 at the 0.001 eV/atom driving force is caused by stick-slip migration, which we now discuss in more detail. To illustrate this stick-slip migration behavior, we have plotted the GB position for one of the two GBs in each simulation as a function of time for the 0.001 eV/atom simulations in Figure 6; the position of both GBs can be seen in supplemental Figures S5-S10. The serrated nature of the GB position vs. time increases with increased solute content and the GBs in some conditions become stuck for long periods of time. This behavior is well-documented [65] and is characterized by sudden motion events interspersed with static periods of varying duration.

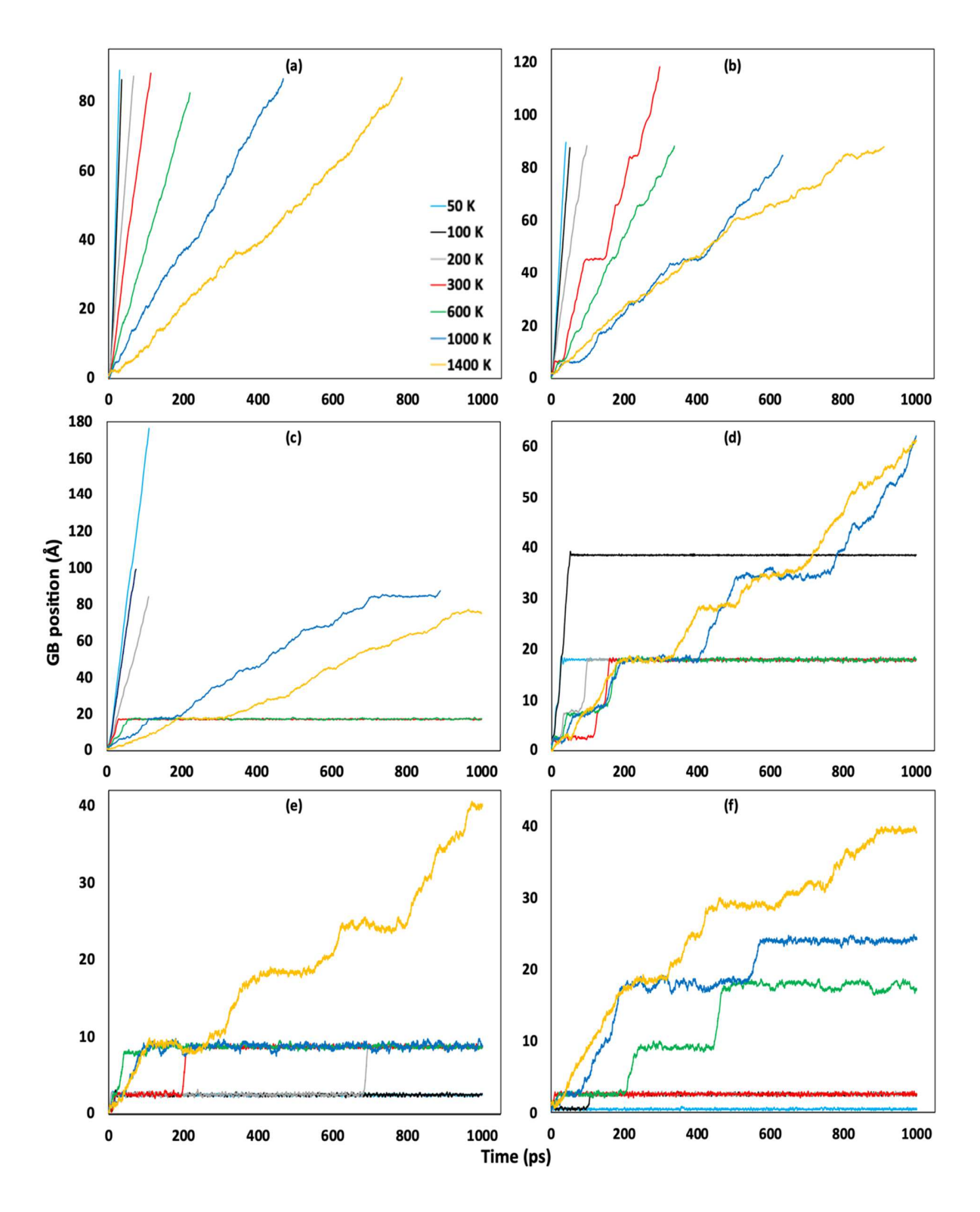


**Figure 6.** Plot showing GB position (Å) vs time period (ps) trends for (a) NiCu0, (b) NiCu2, (c) NiCu4, (d) NiCu6, (e) NiCu8, and (f) NiCu10 configurations at 0.001 eV/atom driving force.

While the tendency for stick-slip behavior increases with increasing solute content, it can also be seen that the highest temperatures suffer from less stick-slip than the lower temperatures. The biggest contrast can be seen in the NiCu0 and NiCu10 plots of Figure 6 for this driving force of 0.001 eV/atom. The NiCu0 exhibits the fastest migration at low temperatures and non-Arrhenius temperature dependence while the NiCu10 exhibits the fastest migration at high temperatures and the migration rate increases with increasing temperature. Thus, with increased solute content at low driving forces, the thermal energy goes from frustrating the migration to facilitating it.

Interestingly, we see no change in the atomic migration mechanisms for simulations that span these transitions, which are illustrated in Figure 7. This lack of a change can be seen for solute contents that exhibit no stick-slip (NiCu0) to one that exhibits stick-slip at nearly every temperature (NiCu10). The relative atomic motions for all solute contents in Figure 7 are nearly identical at any given temperature, except for the 100 and 300 K distributions in the NiCu10 case, which didn't migrate very far and as a result have very few atoms to contribute to the distributions. Supplemental Figure S11 shows that the relative atomic motions for the NiCu4 case are consistent spatially through the simulation cell and that the Ni and Cu atoms exhibit the same distribution of motions. Thus, even when the boundary exhibits this stick-slip behavior, the fundamental atomic motions appear to remain the same.

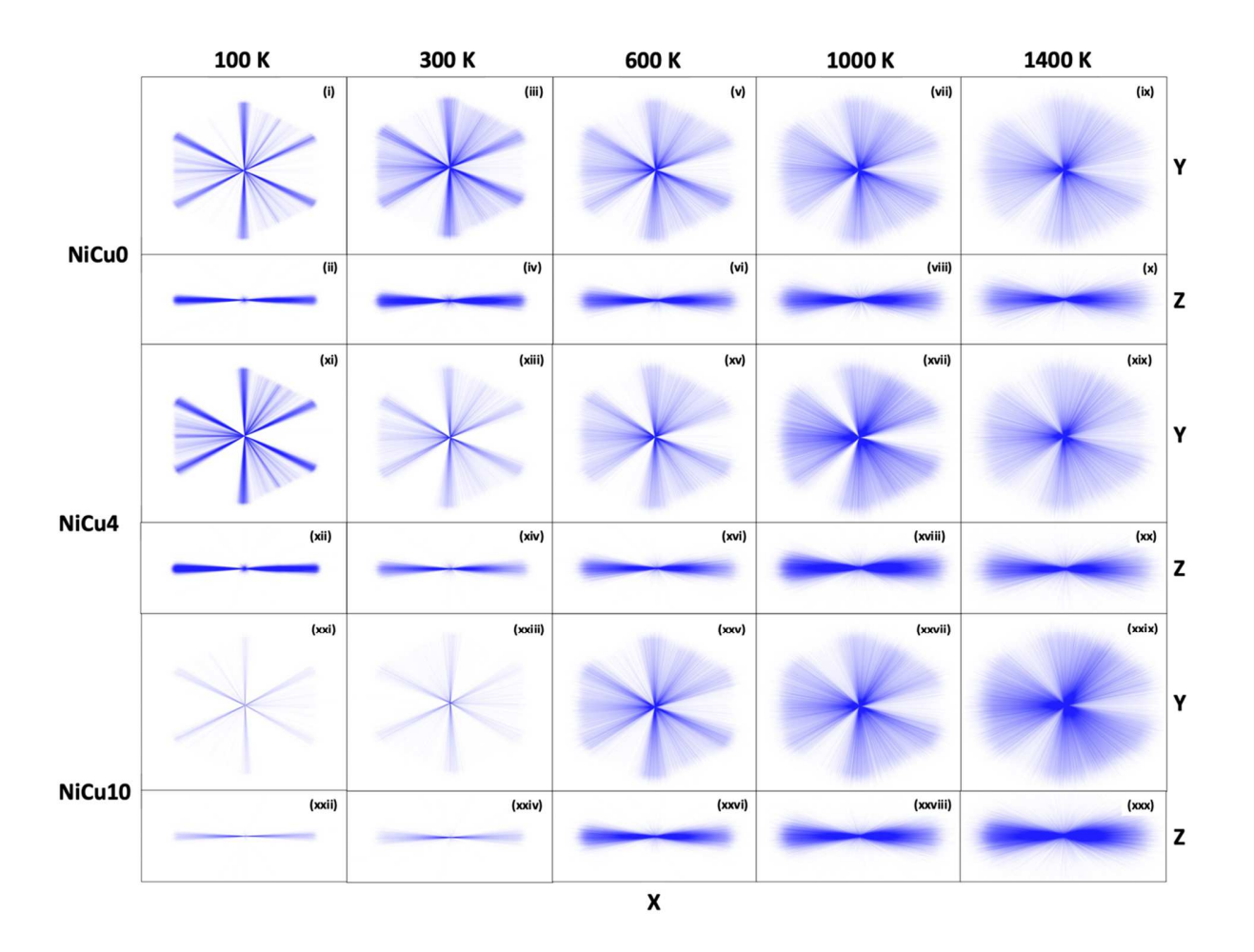


**Figure 7.** Relative atomic motion distributions, calculated from the slip vector, at various temperatures and 0.001 eV/atom driving force for (i-x) NiCu0, (xi-xx) NiCu4, and (xxi-xxx) NiCu10.

Thus, the thermal energy that frustrates the ordered atomic motions at low solute content appears to facilitate the boundary to move out of its 'stuck' state even though the mechanism of motion does not change. The effect of temperature does not change because the mechanism changes from military to civilian motion, rather, the mechanism remains the same, and we see two competing effects of temperature (1) disruption of ordered motion and (2) overcoming the "stuck" state of stick-slip migration. Which one dominates depends on what the rate limiting step

is. At low solute content the rate limiting step is the ordered atomic motions so (1) dominates, but at high solute content sticking becomes rate limiting and so (2) is the dominant effect of temperature.

It is unsurprising that additional thermal energy allows a boundary that exhibits stick-slip motion to migrate more quickly. La et al. suggested that the thermal energy helps to overcome the friction of stick-slip migration [66]. Furthermore, Ulomek and Mohles [9] suggested that the GB migration requires a two-step process of nucleation and migration, and that if temperature or driving force is increased, intermittent GB motion would become smooth again. And Hadian et al. [62] observed stick-slip at comparatively lower temperatures in an aluminum  $\Sigma 7$  GB and found that at higher temperatures, the motion was more continuous.

Interestingly, in Figure 6 the GB often becomes 'stuck' at the same position in the bicrystal even when the temperatures are different. Each of these simulations use the same starting distribution of Cu, which suggests that this distribution likely plays a role. But a comparison of the concentration for the NiCu6 simulations in supplemental Figure S1b with the positions at which the GB gets stuck in Figure 6d shows no correlation to high or low concentrations, nor are these particularly different from other concentrations where the GB does get stuck. There are Cu atoms and even Cu atom clusters in the GB where it is stuck, but these are also in the regions where the

GB has swept through<sup>1</sup>. It is not clear what is special about a given cluster that causes the GB to become pinned. Once pinned, The GB even fluctuates a small amount about the point where it is stuck, so it is not clear which part of the GB is even pinned. Thus, the exact conditions that lead to pinning of the GB are not clear. Nonetheless, the consistency of locations in Figure 6 where GBs do get stuck indicate that there is some dependence on the solute distribution to pinning that can occur.

Having demonstrated the stick-slip behavior and the unchanged nature of the atomic motions, we now examine the role of the solute content on the observed stick-slip behavior. As noted previously, there is a reversal in the temperature dependence between NiCu0 and NiCu10 for the 0.001 eV/atom driving force, which can be seen in Figures 1 and 2. The NiCu0 data follows the trend predicted by equation 3, and therefore exhibits a non-Arrhenius behavior with no stick-slip migration. To illustrate the transition to the behavior in the other extreme of the NiCu10 case, it is helpful to reexamine some of that data.

We begin first with the NiCu6, NiCu8, and NiCu10 data because they are so similar in Figure 1. In Figure 8, we plot the distribution of velocity measurements in a swarm plot, overlaid with a violin plot showing the general shape of the distribution. It is worth noting at this point that the

-

<sup>&</sup>lt;sup>1</sup> The supplemental video shows the boundary migration of the NiCu6 simulation at 600 K and a 0.001 eV/atom driving force. The video has two views of the simulation. The left view is side on and shows only Cu atoms and GB atoms (both Ni and Cu). At 6 at % this still represent a large number of atoms to view making it hard to see how the Cu atoms affect the boundary migration. As a result, the right view is a perspective view and only shows Cu atoms that have more than 2 Cu atoms as nearest neighbors; the GB atoms (both Ni and Cu) are shown as well. It is not clear why some Cu clusters appear to have a more dramatic effect on the boundary migration than others.

uncertainty quantification approach we have adopted is especially helpful in analyzing stick-slip migration since a single fit line to a boundary that exhibits serrated motion would extract a velocity that is not likely to represent that exhibited by the GB at any period. Instead, extracting distributions of velocities allows us to examine the range of values exhibited over short periods of time to see the large number of velocity samples near zero where the boundary is in the 'stuck' state and the relatively few samples where the boundary migrates at higher velocities. At higher temperatures the median velocity increases from zero, but there is a significant variation about the median value. This large uncertainty makes it difficult to state conclusions about the trend with statistical certainty. Nevertheless, the consistent shift in the distributions to higher velocity values with increased temperature, evident in Figure 8, are suggestive of an increasing trend.

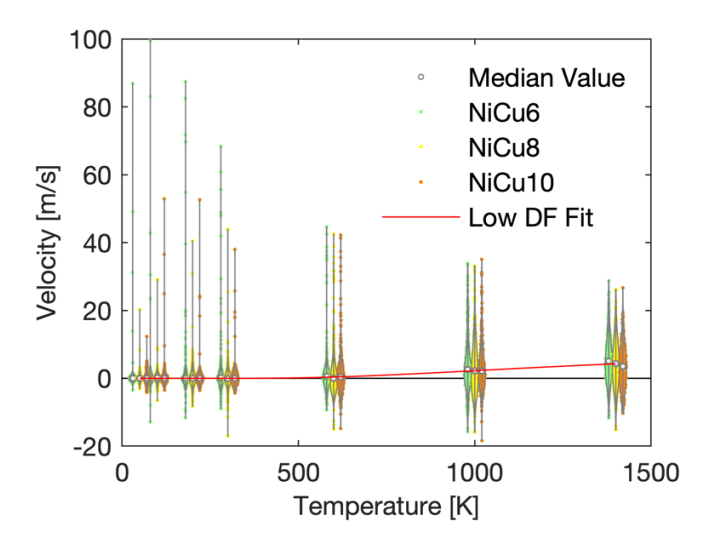


**Figure 8.** GB velocity vs. temperature swarm and violin plots for NiCu6, NiCu8 and NiCu10 alloy configurations at a low driving force of 0.001 eV/atom. The low driving force (DF) curve is fit to the median velocity values of all three alloy configurations. The horizontal black line at v = 0 is included only to guide the eye.

Since the velocities for the NiCu6, NiCu8, and NiCu10 are similar for all three compositions at the 0.001 eV/atom driving force, they were fit together as a single set of data using equation 3. The resulting fit is plotted by the red line in Figure 8. This fit has a Q value of 0.30 eV, which is sufficiently high to predict an Arrhenius temperature dependence. Since this overall trend includes stick-slip behavior, if one believes that it is represented by the Arrhenius fit, the migration barrier, Q, likely includes information about the nucleation energy as well as the migration energy. In fact, given that the migration energy is small when stick-slip is not evident (c.f. Figure 6) and the atomic motions remain the same (c.f. Figure 7), this migration barrier likely represents the energy required for a nucleation event to take the system out of the 'stuck' state and into the 'slip' state since that is what must be overcome for this boundary to continue migrating.

We now examine the NiCu2 and NiCu4 cases, which exhibit some stick-slip behavior, but also some signatures of the non-Arrhenius migration. This data is plotted in Figure 9, along with the fits to the high driving force data that are plotted in Figure 2. The fits are included to show how the data both deviates from and follows the trends that fit the higher driving force data so well. Once again, the velocity distributions provide a chance to see how a boundary can, at times, be stuck for a long period of time but when it migrates, it can migrate at high velocities. The high velocity values decrease with increasing temperature, following the model of the high driving force fits from Figure 2. In short, this data reveals characteristics of the two competing effects of temperature mentioned earlier, (1) disruption of ordered motion and (2) overcoming the "stuck" state of stick/slip. This is key to understanding the transition that occurs between the non-Arrhenius NiCu0 and Arrhenius NiCu6-NiCu10 data. The solute concentrations in these cases

appear to be near the critical values where they will be expected to impact the migration behavior.

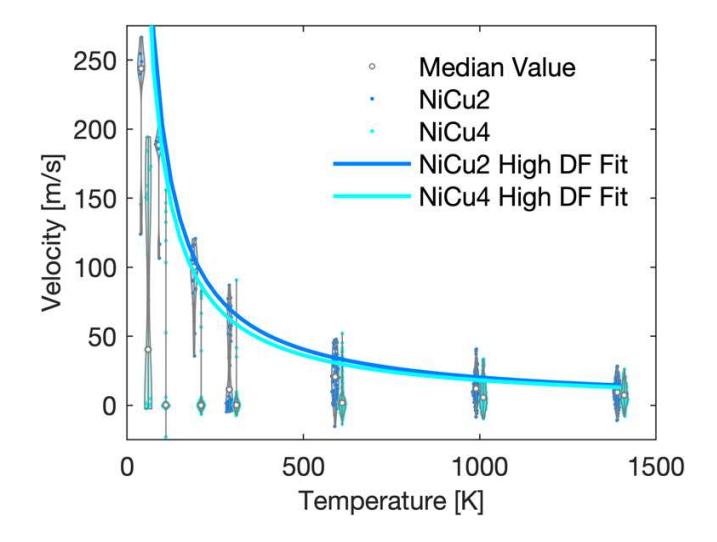


**Figure 9.** GB velocity vs. temperature swarm and violin plots for NiCu2 and NiCu4 alloy configurations at a low driving force of 0.001 eV/atom. The high driving force (DF) curves match the same fit conditions as those in Figure 2.

### 4.4 Implications of solute effects

Figure 1 shows a clear dependence of migration velocity on solute content and the sections above have examined specific aspects of the migration behavior evident in these simulation results. Interestingly, solute content plays a clear role in each of these aspects. The velocity saturation that can occur for fast moving boundaries moves to lower values with increasing solute content and driving force (c.f. Figure 3). The non-Arrhenius behavior seen in many of the simulations can be fit with equation 3 and the fit parameters,  $v_o$  and Q, are dependent upon the solute content (c.f. Figure 4). At the lowest driving force and with increasing solute content, the boundaries exhibit stick-slip motion, which dramatically lowers the boundary velocity (c.f. Figure 6). But additional thermal energy in these cases results in an increase in the median

boundary velocity, presumably because the thermal energy enables the boundary to move out of its 'stuck' state.

It is also instructive to compare our observations with the characteristic behaviors of the CLS model, which models the forces that solute atoms exert on a moving GB [23, 24, 29]. The effect of driving force, solute content, and temperature are readily illustrated in Figure 10 (reproduced from [29]). Figure 10a illustrates how additional solute will slow migration of the boundary, while Figure 10b illustrates how an increased driving force will enable the boundary to break away from the solute and migrate more quickly. In what follows, we examine the two trends predicted by the CLS model illustrated in Figure 10.

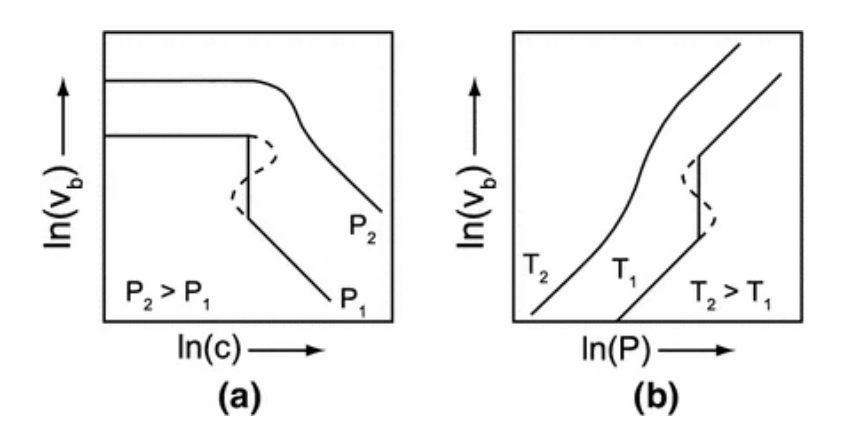


**Figure 10.** Illustration of CLS model and transitions dependent on concentration, driving force, and temperature. Figure adapted and reproduced with permission from [29].

Figure 11 plots the natural logarithm of velocity as a function of the natural logarithm of composition for the three different driving forces at the various temperatures examined in this work. Note that in this graph, negative velocity values present in other graphs have been converted to extremely small positive values that are below the limits shown in the graph. Additionally, the NiCuO data is plotted at a natural logarithm value of 0 instead of negative

infinity. Based on Figure 1a, one would expect a few trends to be evident. First, lower driving forces should lead to lower velocity values, which appears to be true of the data in Figure 11 if the boundary is not exhibiting velocity saturation. Second, increased solute content should lead to a slowing of the boundary velocity regardless of driving force, with more dramatic effects observed at the highest composition values. This is true for all the data shown in Figure 11. Finally, at lower driving forces, one can expect a dramatic drop in boundary velocity at some critical concentration. This is readily apparent in Figure 11 for the lowest driving force and temperatures  $\leq$  600 K at the intermediate solute content values. Interestingly, this drop is not seen at 1000 and 1400 K. But this can be expected because as shown in Figure 10b, the effect of solutes is less dramatic at elevated temperatures.

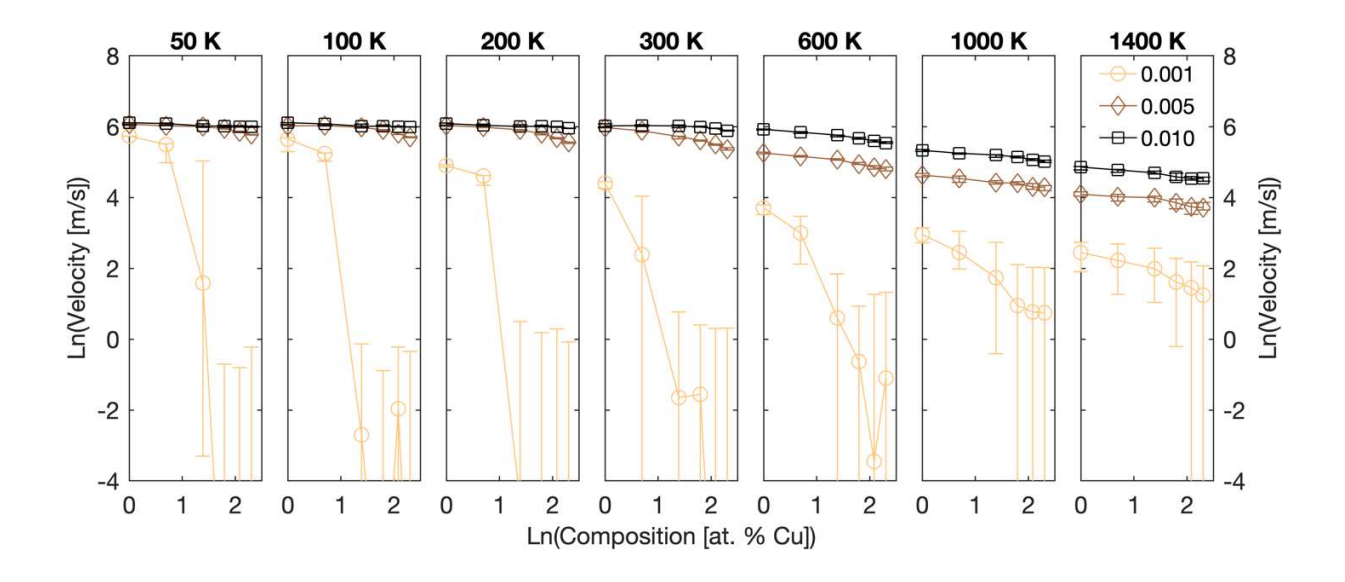


**Figure 11.** Plot of the natural logarithm of velocity vs. the natural logarithm of composition to illustrate solute drag effects as a function of driving force at various temperatures. Negative velocity values in the distribution statistics are set to small positive values below the limits shown in this plot. Note that the NiCu0 values are listed at a natural logarithm value of 0 rather than negative infinity. The legend lists the driving forces in eV/atom.

To examine the temperature trends further, we plot the same data again in Figure 12 as a function of the natural logarithm of driving force for the various temperatures at each of the solute contents. It should be noted that Figure 10b shows the role of temperature under the assumption that boundary migration follows an Arrhenius temperature dependence where higher temperatures lead to faster migration. When a boundary exhibits non-Arrhenius migration, as is the case in many of the simulations in this work, we can expect a reversal of this trend. Thus, the ordering of the velocities in this plot can help us distinguish between Arrhenius and non-Arrhenius, or at least positively and negatively correlated, trends of velocity with temperature. Figure 10b also illustrates that when the boundary breaks away from the solute atoms, one can expect a discontinuous change or larger jump in GB velocity.

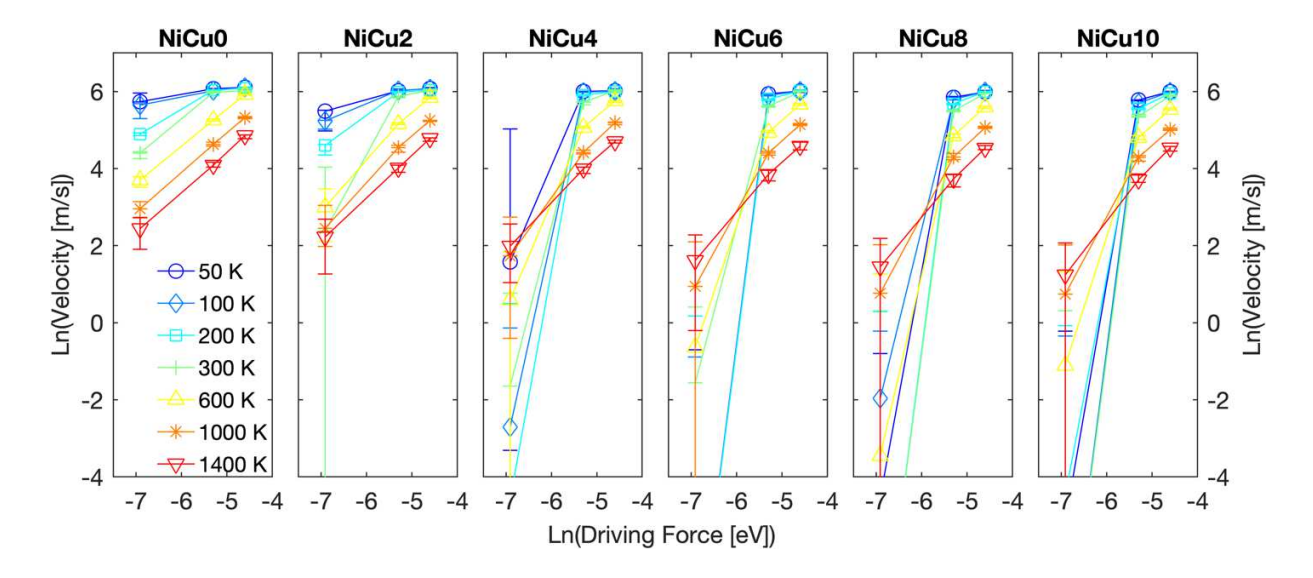


**Figure 12**. Plot of the natural logarithm of velocity vs. the natural logarithm of driving force to illustrate the change in the temperature dependence at the different solute concentrations.

In Figure 12, for the NiCu0 case, the trends are relatively linear with a non-Arrhenius ordering of temperature (i.e., higher velocity values at lower temperatures). But, in the NiCu2 case, at 300 K

and between the 0.001 and 0.005 eV/atom driving forces, there is a larger jump in velocity relative to other temperatures in this plot, indicating some effect from the solute atoms. In examining Figure 7b, one can see that at 0.001 eV/atom and 300 K, the boundary exhibits stickslip behavior. This trend is also evident in the NiCu4 case where a large jump in velocity is seen for the lowest driving forces and intermediate temperatures. Furthermore, the median velocity value for these intermediate temperatures falls below those of the lowest and highest temperatures, which is indicative of a reversal of temperature trends. In other words, as can be seen in Figure 9, the velocity decreases with temperature before increasing again with temperature. The solute effect is therefore dependent on temperature. Also for the NiCu4 case, at low temperatures the solute does impact the migration but to a lesser extent. But as the temperature increases, presence of solute, in combination with the thermal disordering is sufficient to shut down the migration and lead to stick-slip migration. Additional thermal energy then enables the system to move out of the 'stuck' state and spend more time migrating, resulting in an increase in velocity.

In the NiCu6, NiCu8, and NiCu10 cases, the large jump is still seen at the lowest driving forces and the temperature dependence is positively correlated. While the range of values in the distributions, indicated by the error bars for the 1<sup>st</sup> and 3<sup>rd</sup> quartiles, is large, this supports the Arrhenius trend exhibited in Figure 9 for the lowest driving force.

What is particularly interesting about these characteristics of the CLS model is that the solute atoms in this work are never dragged along with the boundary as it migrates. Whereas Koju and Mishin [25] clearly show the effects of solute drag causing the distribution of solute atoms to change, all the solute atoms in the present work remain in their same position in the lattice. This

was confirmed through various measures including mean square displacement of the solute atoms and visualizing their trajectories (through OVITO). As a result, we wish to make clear that while the presence of the solute atoms led to characteristics consistent with the CLS model, we do not observe any solute drag along with the boundary migration. Perhaps the impact of the solute atoms is manifest through the solute pinning effect [29].

An atom with a tendency for segregation, even if it is weak, will have lower energy when that solute is in the boundary, making it more difficult for the boundary to move away. Thus, the boundary could be pinned by the solute atoms and break away even if the solute atoms can never be dragged along with the boundary. This could be the origin of the stick-slip migration instead of the expected solute drag. This is somewhat reminiscent of work that suggested that coincidence site lattice (CSL) atoms could act as pinning sites that frustrated non-Arrhenius GB migration since they were coincident to the two lattices on either side of the boundary [12]. Their simple presence was enough such that when thermal energy was increased, their increased disorder frustrated the coordinated atom motions surrounding the CSL atom. In this same way, solute pinning, due to an energetic interaction of the solute atom with the boundary, may be sufficient to temporarily disrupt the ordered atomic motions or pin the boundary in place for a short period of time.

One could also consider the case where additional annealing prior to migration might allow the solute atoms to segregate to the GB [20]. In these cases, one might expect the traditional solute drag to slow the migration even further in the low driving force cases. But, at the high driving forces one would expect the boundary to break away from any solutes and then sweep through a random solid solution. In this case, one could reasonably expect the migration through the

random solid solution to behave as it is characterized in this work. This has implications for the experimental observation of this phenomenon; high driving forces may be required to induce this effect, which is why the few experiments that suggest that non-Arrhenius GB migration is possible all involved mechanical driving forces [1-6].

Finally, the role of solute is not independent, it is interconnected with the role of temperature and driving force. Because the boundary does not have segregated solute atoms and the atom motions are ordered, it is difficult to directly apply the CLS model to find specific transition points. While one cannot pinpoint exact transition points, the role of driving force is of particular interest because of the role it plays in inducing the migration. It is therefore unsurprising that higher driving forces can induce motion. Among others, both Schratt and Mohles [44] and Deng and Schuh [67] have shown that driving forces of a sufficient magnitude can induce motion, with Schratt and Mohles noting that this can be accomplished for temperatures tending to 0 K as well. The transition observed at low driving forces with increased solute content is consistent with the CLS model and is reminiscent of a recent observation where increasingly small driving forces resulted in a transition of the temperature dependence in the GB migration behavior [50]. In short, in [50] the system appeared to experience a different barrier to migration as the driving force is altered; a fit to the data with equation 3 suggests an increasingly large Q value as the driving force was reduced. Thus, the transition from non-Arrhenius to Arrhenius behavior observed in this work may be the result of combined effects of both solute content and a change in the energetic landscape traversed at lower driving forces.

#### 5 Conclusions

This work demonstrates that the presence of Cu solute atoms in an incoherent Ni twin GB result in migration behaviors that are generally consistent with the Cahn-Lücke-Stüwe (CLS) model. This consistency occurs even in a GB that exhibits non-Arrhenius temperature dependence on the velocity in its pure state. Furthermore, this work is unique in comparison to other examinations of the CLS model because it examines a special boundary, which can exhibit different characteristics than a high angle random boundary, and because the Cu solute in Ni is distributed uniformly in these simulations. Finally, the work can be summarized in the following key points: (i) Holding everything else constant, the increasing presence of solute results in dramatic slowing of the boundary migration.

- (ii) Increasing the driving force results in faster migration, but only to the point that velocity saturation occurs.
- (iii) When non-Arrhenius migration is observed, the basic characteristics of ordered atomic motions and slowing of the boundary by increased thermal disorder remain consistent even in the presence of increased solute content.
- (iv) There is an interaction between solute concentration, driving force, and temperature. As the solute concentration increases and the driving force decreases, there is a fundamental change in behavior from steady motion to unsteady motion (stick-slip). Due to this change, the correlation with temperature changes from negative to positive, resulting in a transition from non-Arrhenius to Arrhenius temperature dependence. However, it is noted that the signal used to measure the Arrhenius dependence is in the noise or scatter of the velocity distributions and there is some

uncertainty in this conclusion. The reason for this change is that the steady motion for these GBs involves coordinated motion so thermal energy frustrates this and decreases the velocity. In contrast, when motion is unsteady thermal energy can enable the GB to overcome obstacles and therefore increases the velocity, or thermal energy can change the structure of the GB (defaceting).

(v) While the results are generally consistent with the CLS model, there is no evidence of solute drag and it is presumed that solute pinning is the source of the solute effects.

#### Acknowledgements

This research work was supported by the U.S. Department of Energy (DOE), Office of Science, Basic Energy Sciences (BES) under the Award #DE-SC0016441. For the final writing and editing, A.V. and S.O. acknowledge the support by JSPS KAKENHI under Grant No. JP22KF0239 and S.O. acknowledges the support by MEXT Programs under Grant No. JPMXP1122684766 and JSPS KAKENHI under Grant No. JP23H00161.

#### **Declaration of Competing Interest**

The authors declare that they have no known competing financial interests or personal relationships that could have emerged to influence the work reported in this article.

# References

- 1. Brons, J.G., Padilla Ii, H.A., Thompson, G.B. and Boyce, B.L., 2013. Cryogenic indentation-induced grain growth in nanotwinned copper. *Scripta Materialia*, 68(10), pp.781-784.
- 2. Brons, J.G., Hardwick, J.A., Padilla II, H.A., Hattar, K., Thompson, G.B. and Boyce, B.L., 2014. The role of copper twin boundaries in cryogenic indentation-induced grain growth. *Materials Science and Engineering: A*, 592, pp.182-188.
- 3. Zhang, K., Weertman, J.R. and Eastman, J.A., 2005. Rapid stress-driven grain coarsening in nanocrystalline Cu at ambient and cryogenic temperatures. *Applied Physics Letters*, 87(6), p.061921.
- 4. Zhang, K., Weertman, J.R. and Eastman, J.A., 2004. The influence of time, temperature, and grain size on indentation creep in high-purity nanocrystalline and ultrafine grain copper. *Applied Physics Letters*, 85(22), pp.5197-5199.
- 5. Frazer, D., Bair, J.L., Homer, E.R. and Hosemann, P., 2020. Cryogenic stress-driven grain growth observed via microcompression with in situ electron backscatter diffraction. *JOM*, 72(5), pp.2051-2056.
- 6. Robinson, J., Verma, A., Homer, E.R. and Thompson, G.B., 2023. Nanotwin stability in alloyed copper under ambient and cryo-temperature dependent deformation states. *Materials Science and Engineering:* A, 871, p.144866.
- 7. Sutton, A.P. and Balluffi, R.W., Interfaces in Crystalline Materials, Clarendon Press, Oxford 1995.

- 8. Homer, E.R., Holm, E.A., Foiles, S.M. and Olmsted, D.L., 2014. Trends in grain boundary mobility: Survey of motion mechanisms. *JOM*, 66(1), pp.114-120.
- 9. Ulomek, F. and Mohles, V., 2016. Separating grain boundary migration mechanisms in molecular dynamics simulations. *Acta Materialia*, *103*, pp.424-432.
- 10. Priedeman, J.L., Olmsted, D.L. and Homer, E.R., 2017. The role of crystallography and the mechanisms associated with migration of incoherent twin grain boundaries. *Acta Materialia*, *131*, pp.553-563.
- 11. Olmsted, D.L., Holm, E.A. and Foiles, S.M., 2009. Survey of computed grain boundary properties in face-centered cubic metals—II: Grain boundary mobility. *Acta Materialia*, *57*(13), pp.3704-3713.
- 12. Bair, J.L. and Homer, E.R., 2019. Antithermal mobility in  $\Sigma 7$  and  $\Sigma 9$  grain boundaries caused by stick-slip stagnation of ordered atomic motions about Coincidence Site Lattice atoms. *Acta Materialia*, 162, pp.10-18.
- 13. Chesser, I. and Holm, E., 2018. Understanding the anomalous thermal behavior of  $\Sigma$ 3 grain boundaries in a variety of FCC metals. *Scripta Materialia*, 157, pp.19-23.
- 14. Homer, E.R., Johnson, O.K., Britton, D., Patterson, J.E., Sevy, E.T. and Thompson, G.B., 2022. A classical equation that accounts for observations of non-Arrhenius and cryogenic grain boundary migration. *npj Computational Materials*, 8(1), pp.1-9.

- 15. O'Brien, C.J. and Foiles, S.M., 2016. Exploration of the mechanisms of temperature-dependent grain boundary mobility: search for the common origin of ultrafast grain boundary motion. *Journal of Materials Science*, 51(14), pp.6607-6623.
- 16. Humberson, J. and Holm, E.A., 2017. Anti-thermal mobility in the  $\Sigma 3$  [111] 60°{11 8 5} grain boundary in nickel: mechanism and computational considerations. *Scripta Materialia*, 130, pp.1-6.
- 17. Turchanin, M.A., Agraval, P.G. and Abdulov, A.R., 2007. Phase equilibria and thermodynamics of binary copper systems with 3 d-metals. VI. Copper-nickel system. *Powder Metallurgy and Metal Ceramics*, 46, pp.467-477.
- 18. Abrikosov, I.A. and Skriver, H.L., 1993. Self-consistent linear-muffin-tin-orbitals coherent-potential technique for bulk and surface calculations: Cu-Ni, Ag-Pd, and Au-Pt random alloys. *Physical Review B*, 47(24), p.16532.
- 19. Iguchi, Y., Katona, G.L., Cserháti, C., Langer, G.A. and Erdélyi, Z., 2018. On the miscibility gap of Cu-Ni system. *Acta Materialia*, *148*, pp.49-54.
- 20. Pellicer, E., Varea, A., Sivaraman, K.M., Pané, S., Surinach, S., Baró, M.D., Nogués, J., Nelson, B.J. and Sort, J., 2011. Grain boundary segregation and interdiffusion effects in nickel–copper alloys: an effective means to improve the thermal stability of nanocrystalline nickel. *ACS Applied Materials & Interfaces*, *3*(7), pp.2265-2274.
- 21. Gottstein, G. & Shvindlerman, L. S. Grain Boundary Migration in Metals. (CRC Press, Boca Raton, 2010).

- 22. Lejček, P. Grain Boundary Segregation in Metals. (Springer-Verlag, Berlin, 2010).
- 23. Cahn, J.W., 1962. The impurity-drag effect in grain boundary motion. *Acta Metallurgica*, 10(9), pp.789-798.
- 24. Lücke, K. and Stüwe, H.P., 1971. On the theory of impurity controlled grain boundary motion. *Acta Metallurgica*, *19*(10), pp.1087-1099.
- 25. Koju, R.K. and Mishin, Y., 2020. Direct atomistic modeling of solute drag by moving grain boundaries. *Acta Materialia*, *198*, pp.111-120.
- 26. Rahman, M.J., Zurob, H.S. and Hoyt, J.J., 2016. Molecular dynamics study of solute pinning effects on grain boundary migration in the aluminum magnesium alloy system. *Metallurgical and Materials Transactions A*, 47(4), pp.1889-1897.
- 27. Sun, H. and Deng, C., 2014. Direct quantification of solute effects on grain boundary motion by atomistic simulations. *Computational Materials Science*, *93*, pp.137-143.
- 28. Sun, H. and Deng, C., 2014. Adapted solute drag model for impurity-controlled grain boundary motion. *Journal of Materials Research*, 29(12), pp.1369-1375.
- 29. Hersent, E., Marthinsen, K. and Nes, E., 2013. The effect of solute atoms on grain boundary migration: A solute pinning approach. *Metallurgical and Materials Transactions A*, 44(7), pp.3364-3375.
- 30. Olmsted, D.L., Foiles, S.M. and Holm, E.A., 2009. Survey of computed grain boundary properties in face-centered cubic metals: I. Grain boundary energy. *Acta Materialia*, *57*(13), pp.3694-3703.

- 31. Fischer, F., Schmitz, G. and Eich, S.M., 2019. A systematic study of grain boundary segregation and grain boundary formation energy using a new copper–nickel embedded-atom potential. *Acta Materialia*, 176, pp.220-231.
- 32. Tschopp, M.A. and McDowell, D.L., 2007. Structures and energies of  $\Sigma$  3 asymmetric tilt grain boundaries in copper and aluminium. *Philosophical Magazine*, 87(22), pp.3147-3173.
- 33. Tschopp, M.A. and McDowell, D.L., 2007. Asymmetric tilt grain boundary structure and energy in copper and aluminium. *Philosophical Magazine*, 87(25), pp.3871-3892.
- 34. Tschopp, M.A. and McDowell, D.L., 2007. Structural unit and faceting description of  $\Sigma$ 3 asymmetric tilt grain boundaries. *Journal of Materials Science*, 42(18), pp.7806-7811.
- 35. Yin, Q., Wang, Z., Mishra, R. and Xia, Z., 2017. Atomic simulations of twist grain boundary structures and deformation behaviors in aluminum. *AIP Advances*, 7(1), p.015040.
- 36. Thompson, A.P., Aktulga, H.M., Berger, R., Bolintineanu, D.S., Brown, W.M., Crozier, P.S., in't Veld, P.J., Kohlmeyer, A., Moore, S.G., Nguyen, T.D. and Shan, R., 2022. LAMMPS a flexible simulation tool for particle-based materials modeling at the atomic, meso, and continuum scales. *Computer Physics Communications*, 271, p.108171.
- 37. Stukowski, A., 2009. Visualization and analysis of atomistic simulation data with OVITO—the Open Visualization Tool. *Modelling and Simulation in Materials Science and Engineering*, 18(1), p.015012.
- 38. Smallman, Raymond Edward. Modern Physical Metallurgy. (Butterworth-Heinemann, Oxford, 2016).

- 39. T.B. Massalski (Ed.), Binary alloy phase diagrams, ASM International, Materials Park, OH (1993).
- 40. Janani, R.D., Salman, S.A., Priyadharshini, K.P. and Karthik, V., 2021. Effect of composition on the stacking fault energy of copper-nickel alloys using molecular dynamics simulations. *Materials Today: Proceedings*, *39*, pp.1796-1800.
- 41. Li, J., Yang, X., Wang, P. and An, Q., 2021. Concentration-temperature superposition principle for grain boundary migration in Ni (Cu) bicrystals. *Materials Today Communications*, 27, p.102464.
- 42. Rupert, T.J., 2014. Solid solution strengthening and softening due to collective nanocrystalline deformation physics. *Scripta Materialia*, 81, pp.44-47.
- 43. Bryukhanov, I.A., 2020. Dynamics of edge dislocation in Cu–Ni solid solution alloys at atomic scale. *International Journal of Plasticity*, *135*, p.102834.
- 44. Schratt, A.A. and Mohles, V., 2020. Efficient calculation of the ECO driving force for atomistic simulations of grain boundary motion. *Computational Materials Science*, 182, p.109774.
- 45. Ulomek, F., O'Brien, C.J., Foiles, S.M. and Mohles, V., 2015. Energy conserving orientational force for determining grain boundary mobility. *Modelling and Simulation in Materials Science and Engineering*, 23(2), p.025007.
- 46. Janssens, K.G., Olmsted, D., Holm, E.A., Foiles, S.M., Plimpton, S.J. and Derlet, P.M., 2006. Computing the mobility of grain boundaries. *Nature Materials*, *5*(2), pp.124-127.

- 47. Johnson, O.K., Homer, E.R., Fullwood, D.T., Page, D.E., Varela, K.F. and Baird, S.G., 2021. Inference and uncertainty propagation of GB structure-property models: H diffusivity in [100] tilt GBs in Ni. *Acta Materialia*, 215, p.116967.
- 48. Zimmerman, J.A., Kelchner, C.L., Klein, P.A., Hamilton, J.C. and Foiles, S.M., 2001. Surface step effects on nanoindentation. *Physical Review Letters*, 87(16), p.165507.
- 49. Homer, E.R., Verma, A., Britton, D., Johnson, O.K. and Thompson, G.B., 2022. Simulated migration behavior of metastable  $\Sigma 3$  (11 8 5) incoherent twin grain boundaries. In *IOP Conference Series: Materials Science and Engineering*, 1249(1), p. 012019.
- 50. Song, X. and Deng, C., 2023. Driving force induced transition in thermal behavior of grain boundary migration in Ni. *Physical Review Materials*, 7(9), p.093401.
- 51. Olmsted, D.L., Hector, L.G., Curtin, W.A. and Clifton, R.J., 2005. Atomistic simulations of dislocation mobility in Al, Ni and Al/Mg alloys. *Modelling and Simulation in Materials Science and Engineering*, 13(3), p.371.
- 52. Akarsh Verma, Oliver K. Johnson, Gregory B. Thompson, Ian Chesser, Shigenobu Ogata, and Eric R. Homer, 2023. Insights into factors that affect non-Arrhenius migration of a simulated incoherent Σ3 grain boundary. *Acta Materialia*, 258, 119210.
- 53. Mishin, Y., Suzuki, A., Uberuaga, B.P. and Voter, A.F., 2007. Stick-slip behavior of grain boundaries studied by accelerated molecular dynamics. *Physical Review B*, 75(22), p.224101.
- 54. Cantwell, P.R., Holm, E.A., Harmer, M.P. and Hoffmann, M.J., 2015. Anti-thermal behavior of materials. *Scripta Materialia*, *103*, pp.1-5.

- 55. Race, C.P., von Pezold, J. and Neugebauer, J., 2014. Role of the mesoscale in migration kinetics of flat grain boundaries. *Physical Review B*, 89(21), p.214110.
- 56. Straumal, B.B., Kogtenkova, O.A., Gornakova, A.S., Sursaeva, V.G. and Baretzky, B., 2016. Review: grain boundary faceting–roughening phenomena. *Journal of Materials Science*, *51*(1), pp.382-404.
- 57. Sursaeva, V.G., Straumal, B.B., Gornakova, A.S., Shvindlerman, L.S. and Gottstein, G., 2008. Effect of faceting on grain boundary motion in Zn. *Acta Materialia*, *56*(12), pp.2728-2734.
- 58. Lee, S.B., Yoon, D.Y., Hwang, N.M. and Henry, M.F., 2000. Grain boundary faceting and abnormal grain growth in nickel. *Metallurgical and Materials Transactions A*, 31(3), pp.985-994.
- 59. Yoon, D.Y. and Cho, Y.K., 2005. Roughening transition of grain boundaries in metals and oxides. *Journal of Materials Science*, 40(4), pp.861-870.
- 60. Straumal, B.B., Polyakov, S.A., Bischoff, E., Gust, W. and Mittemeijer, E.J., 2001. Faceting of  $\Sigma 3$  and  $\Sigma 9$  grain boundaries in copper. *Interface Science*, 9(3), pp.287-292.
- 61. Holm, E.A. and Foiles, S.M., 2010. How grain growth stops: A mechanism for grain-growth stagnation in pure materials. *Science*, *328*(5982), pp.1138-1141.
- 62. Hadian, R., Grabowski, B., Race, C.P. and Neugebauer, J., 2016. Atomistic migration mechanisms of atomically flat, stepped, and kinked grain boundaries. *Physical Review B*, 94(16), p.165413.

- 63. Kirch, D.M., Zhao, B., Molodov, D.A. and Gottstein, G., 2007. Faceting of low-angle < 1 0 0> tilt grain boundaries in aluminum. *Scripta materialia*, 56(11), pp.939-942.
- 64. Kondratev, N.S. and Trusov, P.V., 2017. Influence of orientation grain facets on the migration velocity of high-angle boundaries. In *AIP Conference Proceedings*, 1909(1), p.020088.
- 65. Olmsted, D.L., Foiles, S.M. and Holm, E.A., 2007. Grain boundary interface roughening transition and its effect on grain boundary mobility for non-faceting boundaries. *Scripta Materialia*, 57(12), pp.1161-1164.
- 66. La, S., Liu, C. and Zhang, X., 2019. The mechanism of stick-slip phenomenon during friction process at low temperature environment. *AIP Advances*, *9*(6), p.065019.
- 67. Deng, C. and Schuh, C.A., 2011. Diffusive-to-ballistic transition in grain boundary motion studied by atomistic simulations. *Physical Review B*, 84(21), p.214102.

